*Pure & Appl. Chem.*, Vol. 57, No. 2, pp. 235–246, 1985.
Printed in Great Britain.


# The particle in the box model for resonance Raman scattering in polyacetylene

Hans Kuzmany

Institut für Festkörperphysik der Universität Wien and Ludwig Boltzmann Institut für Festkörperphysik, A-1090 Vienna, Austria

Abstract - The anomalous resonance Raman effect in trans-polyacetylene is described quantitatively by assuming that the conjugations on the polymer chain are statistically interrupted by defects (particle in the box model). The A-term of the Albrecht-theory and the Hückel approximation are used to evaluate the Raman cross section and the optical transition energies and transition moments, respectively. The good agreement with experimental results allowed to determine the distribution function for the defects on the chain. In the second part of the paper the particle in the box model is used to interpret Raman spectra taken during the cis-trans-isomerization, during sample degradation by exposure to air, and during the electrochemical doping process. In the latter case evidence for a reversible order-disorder transition is deduced from the experiments.

## 1. INTRODUCTION

Polyacetylene has been the subject of intensive research work in physics and chemistry for several years (Ref. 1). Initially attention was mainly paid to electrical and magnetic properties of the polymer. More recently the anomalous resonance Raman effect of trans-polyacetylene was studied in detail and valuable information on the structure and the morphology of the polymer was evaluated (Ref. 2-10). The Raman spectrum of the trans-polymer is anomalous since not only the scattering intensity but also the lineshape and the line position of some vibrational modes change with the energy of the exciting laser. This behaviour can be understood from the physical properties of the polyconjugated backbone if defects interrupt the conjugations statistically. In this case the $\pi$-electrons are confined to certain areas of various lengths and behave like particles in the box. The resonance Raman effect of the individual boxes may be expected to be strongly correlated to the resonance behaviour of oligoenes like $\beta$-carotenes and the overall behaviour of the polymer is due to a photoselective resonance process.

In this paper we describe a model which allows a quantitative analysis of experimental results on the basis of a particle in the box system. After a short introduction to the structural properties of the polymer the first part of the paper (chapter 3-7) reviews the basic assumptions and the theoretical background of the model including a comparison with experiments. Very good agreement between experimental and calculated results is observed. Thus in the second part of the paper (chapter 8) applications of the model to problems in physics and chemistry of polyacetylene are reviewed. According to the good understanding of the experiments resonance Raman scattering is now becoming one of the key experimental techniques in the field. In particular the irreversible cis-trans-phase transition (Ref. 8) and the reversible metal-insulator phase transition (Ref. 11) have been studied recently and a direct relation between Raman lineshape and conductivity was established (Ref. 12).

## 2. STRUCTURE OF POLYACETYLENE

If polyacetylene is polymerized at low temperatures (-80°C) the metastable cis-geometry of the backbone shown in Fig. 1A is obtained. Baking the polymer even for a short time at elevated temperatures leads to a transition to the trans-geometry shown in Fig. 1B. In both cases the $sp_2$ hybridized orbitals of the carbon atom undergo $\sigma$-bonding to nearest neighbours whereas the $2p_z$-orbital generates a fairly broad ($\sim$12 eV) onedimensional $\pi$-electron band. Bond alternation as a consequence of a Peierls distortion splits the $\pi$-band and opens a gap of 1.4 and 1.8 eV for the trans- and the cis-isomer, respectively. The lower half-band is filled with electrons (valence band) and the upper half-band is empty (conduction band). Thus, due to spontaneous symmetry breaking on the chain polyacetylene is a Peierls insulator. Using a Ziegler-Natta catalyst for the polymerization (Ref. 13) thin films with 75-90% X-ray crystallinity and a fibrillar structure with a fiber diameter of 200 to 500 Å are obtained (Ref. 14). The chain axis is parallel to the fiber axis (Ref. 15). The X-ray scattering coherence length for trans-polyacetylene was found 70-90 Å and 100-130 Å for directions perpendicular and parallel to the chains, respectively (Ref. 16). From very recent X-ray and $C^{13}$-NMR experiments the bond alternation in the trans-polymer was determined to be 0.03 Å (Ref. 16, 17).

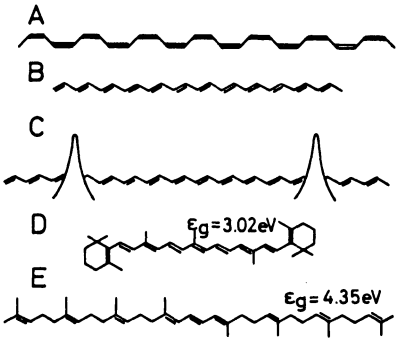


Fig. 1. Geometry of macromolecules : A cis-polyacetylene, B transpolyacetylene, C interrupted conjugation, D septapreno β-carotene, E transphytoene.

The description of the polymer as a nominally perfect crystal must be taken with some care particularly for the trans-isomer. To understand its properties it is rather recommended to consider a distribution of segments of undisturbed conjugations along the chain as shown in Fig. 1C. The nature of the interruption will be discussed later. For long segments the solid state limit will apply (Ref. 18) but in short segments the discreteness of the band states becomes reasonable. In that sense polyacetylene is a nice example for a continuous transition from a molecule to a solid. The effect of interrupting conjugations on physical properties of the chain can be demonstrated by comparing e.g. optical transition energies of septapreno β-carotene and trans-phytoene as shown in Fig. 1D and E. Both oligoenes have 9 double bonds. However, in trans-phytoene the length of undisturbed conjugations (box length) is much smaller and thus the transition energy from the highest occupied to the lowest unoccupied molecular orbital is much larger. Vibrational symmetry species for the cis-polymer evaluated for 4 CH-units per unit cell and $D_{2h}$ symmetry on the chain are

$$\Gamma = 4A_g + B_{1g} + 4B_{2g} + 2A_u + 3B_{1u} + B_{2u} + 3B_{3u}$$

Similarly, for the trans-polymer with 2 CH-units per unit cell and $C_{2h}$ symmetry on the chain

$$\Gamma = 4A_g + 5B_g + A_u + 2B_u$$

In the following only the trans-isomer will be considered. Its Raman spectrum has 5 characteristic lines at 1008, 1100, 1170, 1290, and 1500 $cm^{-1}$, respectively. The two lines at 1100 and 1500 $cm^{-1}$ are strongly resonance enhanced and show the anomalous Raman effect described above. Since only the one with the high frequency has a simple bond stretching normal coordinate, the particle in the box model will only be applied and discussed for this mode though actually it holds similarly for the lower frequency mode as well.

## 3. EXPERIMENTAL RESULTS ON TRANS-POLYACETYLENE

If not specified explicitely all results shown below were obtained with a standard Raman spectrometer at nominally liquid nitrogen temperature. Intensities were calibrated using the 328 $cm^{-1}$ line of $CaF_2$ and the emission of an Osram Wi17/G tungsten lamp. Fig. 2A shows the photoselective resonance behaviour for the C=C stretch mode of a standard sample of trans-polyacetylene. Changing the wave-length of the exciting laser from deep red to purple leads to a substantial line broadening and line shift from about 1460 $cm^{-1}$ to typically 1520 $cm^{-1}$ with a broad shoulder extending to 1540 $cm^{-1}$ (Ref. 5). Spectra are normalized to equal height. For deuterated trans-polyacetylene this effect is even more pronounced and a total shift of 140 $cm^{-1}$ has been observed. In both cases this shift covers rather exactly the frequency range observed for the C=C stretch mode in oligoenes with conjugation lengths varying from very small values to nominally infinity (Ref. 5). For samples polymerized and isomerized under special care the line shape changes substantially as shown in Fig. 2B. Particularly for spectra excited in the blue and purple spectral region a double peak structure develops. As will be shown below in detail the sharp low frequency peak is due to the crystalline part of the polymer with long undisturbed conjugations. The high frequency peak comes from the short segments in amorphous areas. The lineshape of the C=C stretch mode as excited with the 4579 Å laser line is now widely used as a standard to characterize sample quality. Lower scattering intensity at the 1500 $cm^{-1}$ band refers to less defects interrupting the conjugations.

Since the lineshape changes dramatically with excitation energy a simple excitation profile can not be determined. However, plotting the intensity of a particular Raman shift as a function of the energy of the exciting laser a diagram similar to an excitation profile can be obtained for the various Raman shifts. Fig. 3 shows a result for a high quality sample. The Raman cross section is plotted in arbitrary units. Open symbols are as obtained in our experiments (Ref. 19). Intensities have been corrected for absorption and reflection and for spectrometer sensitivity. Full symbols are as reported by Lauchlan et al. (Ref. 20). These data were multiplied by a constant factor to scale to our results. Full drawn lines are as calculated from the particle in the box model described below.

## 4. THE PARTICLE IN THE BOX MODEL

In the particle in the box model the trans-polymer is assumed to consist of a distribution

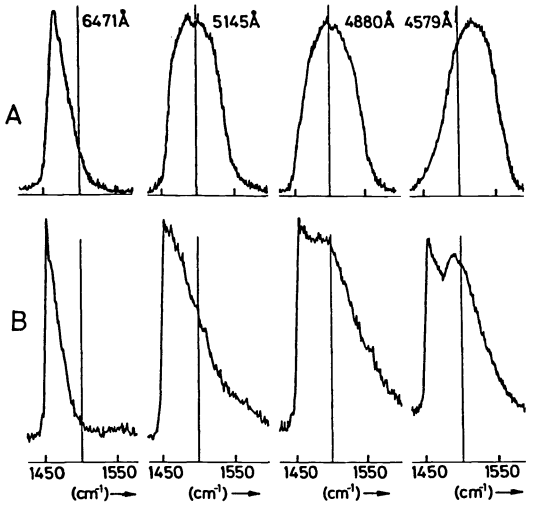


Fig. 2. Resonance Raman effect for the C=C stretch mode in trans-polyacetylene A standard sample, B high quality sample.

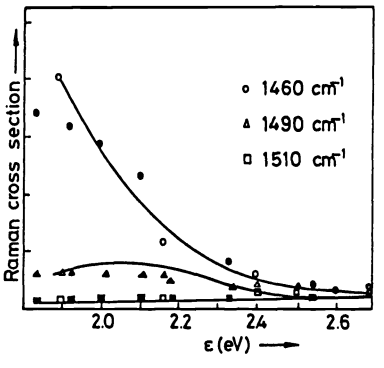


Fig. 3. Raman cross section for the C=C stretch mode in transpolyacetylene. Open symbols (Ref. 19), full symbols (Ref. 20), lines as calculated from Eq.(8).

P(N) of segments with undisturbed conjugations of N double bonds. Thus evaluating the scattering intensity for the individual segments and weight averaging the result according to P(N) should yield the lineshapes and line intensities observed in the experiment for the various exciting laser lines. The scattering cross section $(d^2\sigma/d\Omega d\omega)_{m,n}$ for a transition between an initial state m and a final state n is given by

$$\left(\frac{d^2\sigma}{d\Omega d\omega}\right)_{m,n} = \frac{2\,\omega_s^3}{3^2 c^4\,\hbar} \sum_{\rho,\sigma} \left|(\alpha_{\rho\sigma})_{m,n}\right|^2 \tag{1}$$

where $\omega_s$ is the angular frequency of the scattered light, $(\alpha_{\rho\sigma})_{m,n}$ is the $\rho\sigma$-component of the polarizability and the intensity of scattered light is given in counts per second. For an electronically highly anisotropic system like the chains of polyacetylene the component of $\alpha_{\rho\sigma}$ parallel to the chain axis will dominate which allows to restrict the evaluation to $(\alpha_{zz})_{m,n}$. The transition polarizability is obtained from second order perturbation theory in the dipol version

$$(\alpha_{zz})_{m,n} = \sum_e \left[\frac{\langle m|R_z|e\rangle\langle e|R_z|n\rangle}{(\varepsilon_e - \varepsilon_m) - \varepsilon_o} + \frac{\langle m|R_z|e\rangle\langle e|R_z|n\rangle}{(\varepsilon_e - \varepsilon_m) + \varepsilon_o}\right] \tag{2}$$

where the sum is over the total of intermediate states, $R_z$ is the z-component of the total electronic dipol moment and $\varepsilon_o$ is the energy of the exciting laser (Ref. 21). Assuming the states m, n, and e as adiabatic Born-Oppenheimer states gi, gj, and ev with the energies $\varepsilon_{gi}$, $\varepsilon_{gj}$, and $\varepsilon_{ev}$, respectively, and applying a Herzberg-Teller expansion for the electronic wave functions yields $\alpha_{zz}$ expressed in the A, B, and C-term of the Albrecht theory. For the case of resonance the A-term is regarded as sufficient to describe the scattering intensity whereas for preresonance the B-term has to be included (Ref. 22). For the calculation of Raman lineshapes of trans-polyacetylene so far only the A-term has been used. Thus, considering only the resonance part $\alpha_{zz}$ yields

$$(\alpha_{zz})_{gi,gj} = \sum_e{}' \sum_v \frac{\langle g^o|R_z|e^o\rangle^2\,\langle i|v\rangle\langle v|j\rangle}{(\varepsilon_{ev} - \varepsilon_{gi}) - \varepsilon_o} \tag{3}$$

The electronic transition matrix element $\rho_{ge} = \langle g^o|R_z|e^o\rangle$ is evaluated for the equilibrium geometry whereas in the vibronic matrix elements $\langle i|v\rangle$ and $\langle v|j\rangle$ $\langle i|$ and $\langle j|$ are ground state harmonic oscillator wave functions and $\langle v|$ is the factorized excited state oscillator wave function. It is described in terms of the dimensionless Franck-Condon vibrational coupling constant a or by the displacement of the excited state harmonic oscillator $\Delta q$

$$\Delta q = a\left(\frac{h}{4\pi^2\,m\,f}\right)^{1/2} \tag{4}$$

where m is the reduced mass of the oscillator and f is its frequency in $sec^{-1}$. For first order Raman scattering i = 0 and j = 1. In this case Eq.(3) can be rewritten in the form

$$(\alpha_{zz})_{0,1} = \sum_I \rho_{ge}^2 \sum_v \frac{\langle 0|v\rangle \langle v|1\rangle}{\varepsilon_{Iv} - \varepsilon_o + i\,\Gamma_e/2} \tag{5}$$

where $\varepsilon_{Iv} = \varepsilon_{ev} - \varepsilon_{gi} = \varepsilon_I + \sum_k \hbar\omega_k v_k$. $\varepsilon_I$ is the pure electronic transition energy. The sum over v includes all optical phonons with angular frequency $\omega_k$ and occupation numbers v from 0 to infinity. In Eq.(5) a phenomenological full width half maximum damping constant $\Gamma_e$ describing the lifetime of the excited state was added. For the vibrational mode s the Franck-Condon integral in Eq.(5) becomes

$$\langle 0|v\rangle \langle v|1_s\rangle = \frac{(a_s^2/2)^{v_s - \frac{1}{2}} (v_s - a_s^2/2)}{\prod_{i\neq s} 2^{v_i} v_i !} \prod_{i\neq s} a_i^{2v_i} \exp\left(-\sum_i (a_i^2/2)\right) \tag{6}$$

This equation shows that only modes with a reasonably large Franck-Condon coupling constant $a_i$ contribute to the resonance effect. Thus evaluating the susceptibility from Eq.(5) only the two strongly resonance enhanced modes around 1100 and 1500 $cm^{-1}$ have to be considered. Also, since in trans-polyacetylene the $a_i$ are smaller than 1 the Franck-Condon integrals decrease rapidely with increasing v which allows to neglect large vibronic occupation numbers. Eq.(5) gives the transition polarizability for a particular segment. The quantities $\varepsilon_I$, $\rho_{ge} = \rho_I$, $\Gamma_e$, and $a_i$ are characteristic functions of the number of double bonds N in the segment. Using the evaluated transition polarizabilities $\alpha_{zz}(N)$ the total Raman cross section is obtained from Eq.(1) if the individual contributions are weightened by the distribution function P(N) and a Lorentzian lineshape

$$L(\nu,N) = \frac{\frac{1}{2\pi}\Gamma_p(N)}{(\nu-\nu_2(N))^2 + (\Gamma_p(N)/2)^2} \tag{7}$$

where $\nu$ is the Raman frequency in wave numbers. Again the damping constant $\Gamma_p$ and the C=C stretch frequency $\nu_2$ are characteristic functions of N. The final relation for the Raman lineshape yields

$$I(\nu,\varepsilon) = C \sum_N P(N) |\alpha_{zz}(N)|^2 \omega_s^3 L(\nu,N) \tag{8}$$

where C is a constant. This equation describes quantitatively experimental lineshapes and line intensities for any laser line $\varepsilon_o$ if the experiment is properly corrected for absorption and reflection. It should be stressed that P(N) is a distribution of segments and not the fraction of the polymer material in segments with a particular length N. This quantity is rather given by N×P(N).

## 5. PHYSICAL PROPERTIES FOR THE INDIVIDUAL SEGMENTS

To evaluate Eq.(8) explicitly the relations $\varepsilon_I(N)$, $\rho_I(N)$, $\nu_2(N)$ etc. must be known. The electronic transition energies $\varepsilon_I(N)$ and transition moments $\rho_I(N)$ can be evaluated from a Hückel calculation (Ref. 23). In this case the bond alternation is described by transfer integrals $\beta_n$ which take the values $\beta_1$ and $\beta_2$ for the single and double bond, respectively. Accordingly the Hückel Hamiltonian

$$H = \sum_{n,s} \beta_n (a^+_{n,s} a_{n+1,s} + a^+_{n+1,s} a_{n,s}) \tag{9}$$

must be diagonalized using molecular orbitals $\psi_i = \sum_k c_{ik}\chi_k$ where $\chi_k$ are the $2p_z$ atomic orbitals. From the eigenvalues of H the transition energies for vertical and symmetry allowed transitions between occupied and unoccupied states can be obtained. The numerically evaluated results for $\varepsilon_I(N)$ may be interpolated for convenience from the relation

$$\varepsilon_I(N) = 2\left[\beta_1^2 + \beta_2^2 + 2\beta_1\beta_2 \cos\pi\left(\frac{N+1-I}{N+1-A(I)}\right)\right]^{1/2} \tag{10}$$

where A(I) is a fitting parameter of the order of one. For the first four transitions it has the values 1.5, 3, 4, 6, respectively. It should be mentioned that the transition energies evaluated here do not rely on periodic boundary conditions. Thus they are valid for very short and long segments simultaneously. The values for $\beta_1$ and $\beta_2$ may be chosen to give the correct bond length for the single bond and the double bond, respectively and the correct absorption energies for finite polyenes or to give the correct total band width. In both cases the gap energy for the infinite long segment $2(\beta_1-\beta_2)$ should be 1.4 eV. In a simplified version for the treatment of the problem it may be sufficient to consider only the lowest energy $\pi$-$\pi^*$ transition. In this case a simplified relation (Ref. 24) of the form

$$\varepsilon(N) = h^2(2N+1)/32\, m_o N^2 a^2 + V_o\,(2N-1)/2N \approx V_o + h^2(16\, m_o a^2)^{-1}/N \tag{10a}$$

may be used.

The electronic transition matrix elements $\rho_I(N)$ may be evaluated on the Hückel level as well using either the dipol approach or better the momentum approach.

$$\rho_I(N) = \sqrt{2}\,\frac{\hbar}{m_o}\,\langle\psi_g|\frac{\partial}{\partial x}|\psi_e\rangle/\varepsilon_I \qquad (11)$$

The transition matrix elements show a rapid increase with N for N≦30. Above this value the relation $\rho_I(N)$ becomes fairly flat and the matrix elements finally approach a constant. Up to 150 double bonds the behaviour of $\rho_I(N)$ is well described by a potential law (Ref. 23). For the simplified treatment of the problem again the Hückel results for the lowest π-π* transition may be replaced by a simple relation. $\rho_I \propto N^{1/2}$ for N≦30 and constant for N>30 will be a good approach in this case.

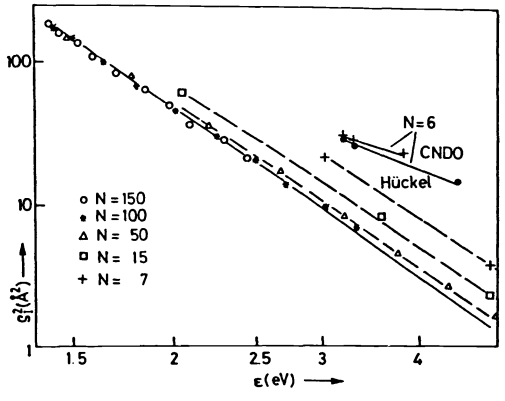


Fig. 4. Square of electronic transition moment $\rho_I^2$ versus transition energy ε for various segment lengths N. The lines CNDO and Hückel correspond to a 30° twist on a segment with N=6.

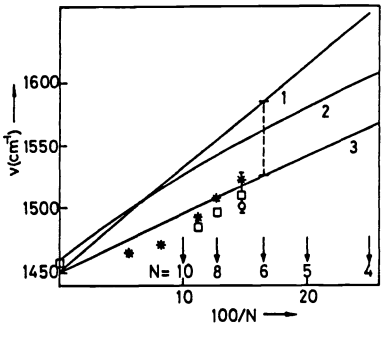


Fig. 5. C=C stretch frequency versus segment lengths. 1 carotenoids (Ref. 25), 2 carotenoids dicarboxylic ester polyenes (Ref. 2,4), 3 average of various oligoenes (Ref. 9). Symbols are from polyacetylene.

With increasing transition energy $\rho_I(N)$ decreases rapidly, no matter whether the increase in transition energy is due to constant values of N and increasing values of I or constant values of I and decreasing values of N. This behaviour is documented by Fig. 4 where we have plotted $\rho_I^2$ as a function of the transition energy. The full drawn line is $1/\varepsilon^4$. The behaviour even holds, if the transition energy is increased by introducing a special type of defect to the chain as shown by the lines in the upper right part of the figure. In these cases the transition energies and transition moments were calculated on the Hückel level or on the CNDO level for a 30° twist of the chain. The general and from N and I independent relation between $\rho_I$ and ε for long segments is typical for the solid state limit.

The relation between vibrational frequency $\nu_2$ and segment length N can be obtained from a study of finite polyenes. Relation of the form

$$\nu_2 = A_2 + B_2/N \quad \text{or} \quad \nu_2 = A_2 + B_2/(N+1) \qquad (12a)$$

for the C=C stretch mode and

$$\nu_1 = A_1 + B_1/N \qquad (12b)$$

for the mode at 1100 $cm^{-1}$ may be used. Depending on which series of oliogenes is considered, $B_2$ may vary from 820 to 460 $cm^{-1}$ and $A_2$ from 1450 to 1460 $cm^{-1}$. Fig. 5 shows relations according to Eq.(12a) for various oligoenes. A rough estimate for the relation between $\nu_2$ and N may be obtained directly from the experiment if the photoselective resonance is assumed to dominate the lineshape. The peak position of the Raman line for the C=C stretch mode is then determined by the particular segment for which the laser energy matches the gap energy. Thus, using Eq.(10) the corresponding segment length can be determined. The symbols in Fig. 5 refer to experimental results obtained in this way for various samples. The error bar reflects the scattering of experimental results and thus characterizes the influence of the sample specific distribution function on the line position.

For the N-dependence of the coupling constants $a_i$ between the electronic and vibronic states an extrapolation of experimental results obtained by Granville et al. (Ref. 26) for several oligoenes up to dodecahexaene may be used. In the corresponding work a Franck-Condon analysis of optical absorption is used to obtain normal coordinate displacement ΔQ and bond length change Δr in the form

$$\Delta Q = \Delta r\,(cmN/2h)^{1/2} = a\,(\nu/N)^{1/2} \qquad (13)$$

where c is the light velocity and ν is the mode frequency in wave numbers. These results yield for the 1500 $cm^{-1}$ and the 1100 $cm^{-1}$ mode, respectively

$$a_2(N) = C\,(1 + \frac{9.5}{N}) \tag{14a}$$

$$a_1(N) = \frac{C}{2}\,(1 + \frac{9.5}{N}) \tag{14b}$$

The dependence of the damping constants $\Gamma_e$ and $\Gamma_p$ on N are obtained from linear interpolations of the form

$$\Gamma_{p,e} = A_{p,e} + B_{p,e}/N \tag{15}$$

## 6. COMPARISON WITH EXPERIMENTS

For a comparison between experimental results and model calculation we have used Eq.(8) together with the equations described in section 5. For P(N) usually a bimodal log-normal distribution function of the form

$$P(N) = \sum_{i=1,2} \frac{F_i}{\sqrt{\pi}\,\Delta_i\,N} \exp\,(-(\ell n^2(N/N_i))/\Delta_i^2) \tag{15}$$

was used where $\Delta_i$ and $N_i$ characterize the widths and the peak values of the individual distributions and the $F_i$ determine their relative weight. The distribution function was cut at N=3 and N=150 for convenience and the physical properties were evaluated for this range of segment lengths. Other distribution functions like Gaussians were shown to give similar results (Ref. 18). To obtain a good fit of the calculated line shapes and line intensities for a high quality sample the parameters given in Tab. 1 have been used.

TABLE 1. Parameters to evaluate Raman line shapes for the C=C stretch mode of a high quality trans-polyacetylene sample

| P(N) | | | $\nu_1(N)$ | $\nu_2(N)$ | $\Gamma_p(N)$ | $\Gamma_e(N)$ | a(N) |
|---|---|---|---|---|---|---|---|
| $F_1$=0.6 | $N_1$=10 | $\Delta_1$=0.8 | $A_1$=1050 | $A_2$=1450 | $A_p$=6 | $A_e$=1200 | C=0.2 |
| $F_2$=0.4 | $N_2$=50 | $\Delta_2$=0.4 | $B_1$= 350 | $B_2$= 460 | $B_p$=360 | $B_e$=-1800 | |

To check the agreement between experiment and calculation it is sufficient to compare some individual lineshapes as shown in Fig. 6. Correction for absorptions and reflections was obtained by multiplying the calculated spectra with

$$\frac{(1 - R_i)\,(1 - R_s)}{K_i + K_s} \approx \frac{(1 - R)^2}{2K}$$

where R and K are the reflection and absorption coefficients as obtained from optical data reported by Fincher et al. (Ref. 27). These correction factors scale from 1 to 1.6 for a transition from red to blue laser light. Intensities for calculated and measured spectra were matched only for the peak position of the red laser excitation The general good agreement strongly supports the interpretation of the anomalous Raman effect as a photoselective resonance process and justifies the particle in the box model for a quantitative interpretation of the lineshapes. From the parameters in Tab. 1 we may obtain the distribution of material on the various segments. Accordingly Fig. 7 shows NP(N) as a function of N. The distribution is dominated by a broad peak around 50 double bonds and shows a second smaller peak around 10 double bonds. These peaks may be interpreted as coming from the crystalline and amorphous parts of the sample. 50 double bonds correspond to a total coherence length of 140 Å in excellent agreement with results from X-ray scattering. Since for segments longer than 40 double bonds the physical properties merge into the solid state limit and thus can not be discriminated any more it is useful to plot the amount of material M(N) in segments longer than N as a function of N. This quantity is obtained from P(N) by

$$M(N) = \sum_{N'=N}^{Nmax} N'P(N') \Big/ \sum_{N'=Nmin}^{Nmax} N'P(N') \tag{16}$$

The result is plotted in Fig. 7 as broken line. If the break between amorphous and crystalline material is somewhere between 10 and 20 double bonds 75 % to 90 % of the material is in crystalline areas again in agreement with X-ray results.

Eq.(8) also allows to calculate the excitation profile shown in Fig. 3, if $\nu$ is kept constant and $\varepsilon_0$ varies over the visible range. The full drawn lines in the figure are results of a similar but slightly simplified version of the calculation. Again satisfactory good agreement between calculation and experiment is obtained.

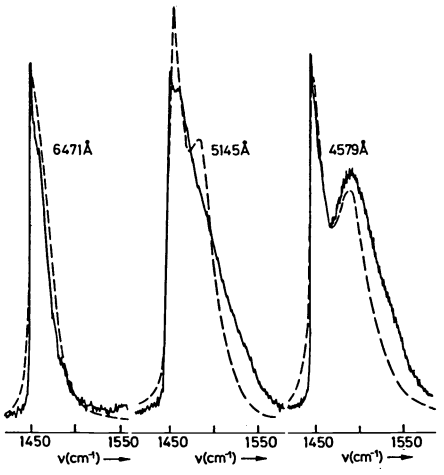


Fig. 6. Comparison of experimental results (calibrated intensities) of the Raman line for the C=C stretch mode of trans-polyacetylene with calculations from Eq.(8).

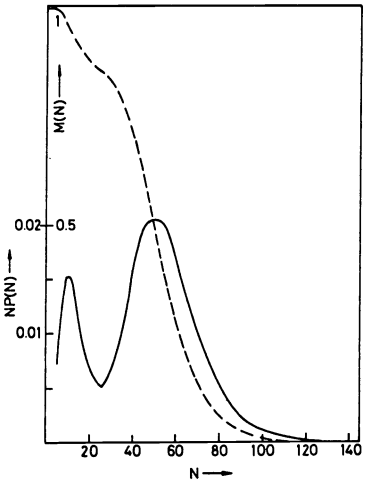


Fig. 7. Distribution N P(N) (full drawn line) and total amount M(N) of polymer material (dashed line) versus N for the sample of Fig. 6.

The parameter values for $\Gamma_p$ and $\Gamma_e$ need some discussion. $A_p$ is the damping constant in units of $cm^{-1}$ for very long segments. Its value is well defined by the very steep low frequency edge of the Raman lines. The high value of $B_p$ would yield a damping constant of e.g. 66 $cm^{-1}$ for N=6. This large value is definitely not due to a life time but rather due to an inhomogeneous broadening. As can be seen from the dashed line in Fig. 5 it correlates indeed well with the range of vibrational frequencies expected for polyenes with various end groups. The parameters for $\Gamma_e$ yield 1200 $cm^{-1}$ and about 600 $cm^{-1}$ for the long and very short segments, respectively. The large values for the long segments may be due to better relaxation channels in these segments (Ref. 28)

## 7. VIOLATION OF THE q-SELECTION RULE AND NATURE OF DEFECTS

Though there is general good agreement between the calculated and observed results some details of the experiments are not well represented. The discrepancy in line intensities is e.g. likely due to an error in the calibration of the spectrometer which is a serious problem for the broad spectral region considered. The disagreement of observed and calculated widths of the Raman lines is also a general experience. It is probably due to an insufficient consideration of the range of vibrational frequencies for a particular segment length. The range may be larger than pointed out in Fig. 5. In addition the selection rule for momentum conservation in the scattering process will be more and more violated for shorter segments because the wave vector q is not a good quantum number any more. Thus modes with $q \neq 0$ will contribute to the scattering process. From the dispersion relation vibrations with increasing q have increasing frequencies and may thus also cause a line broadening. A classical treatment of the problem showed that this effect can contribute to the lineshape for segment lengths between 8 and 15 double bonds which is just the range which determines the high frequency part of the Raman lines. A contribution from shorter segments is prevented by the discreteness of the q-vectors and a contribution from longer segments by the validity of the q-selection rule.

Very little is known about the structure of the defects interrupting the conjugation. Fig. 8 shows some examples. Carbonyl groups (A), hydroxyl groups (B) or similar side groups will definitely interrupt the conjugations in the sense shown in Fig. 1. Also a simple cross link (C) or a Diels-Adler cross link (D) will cause a complete interruption of the π-electron system. Other defects like a single locked in cis-segment (E) or a chain fold (F) may not separate two segments completely. Similarly chain bending, chain twisting or polarization effects (G) may act as weak interruptions of conjugations. Finally, a trapped or untrapped bond alternation defect (soliton) (H) may be considered as a chain defect. However, since solitons tend to delocalize the π-electrons they will probably not interrupt conjugations in the sense of Fig. 1.

The question for the magnitude of an interruption necessary to completely cut a segment into two pieces may be put forward. From a very simple particle in the box study the principle answer can be given as shown in Fig. 9 (Ref. 29). The energies of the states are plotted as a function of a perturbing potential $V = V_o\delta(x - x_o)$ at a position $x_o$ in a box ranging from -a to +a. As can be seen, even small perturbations leed to an increase of the energies and thus to an increase of the transition energies until finally, after complete interruption of the

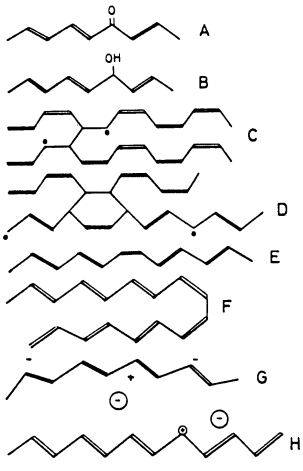


Fig. 8. Possible chain defects: A carbonyl group, B hydroxyl group, C simple cross link, D Diels-Adler cross link, E quenched in cis-segment, F chain fold, G chain bending, H trapped soliton.

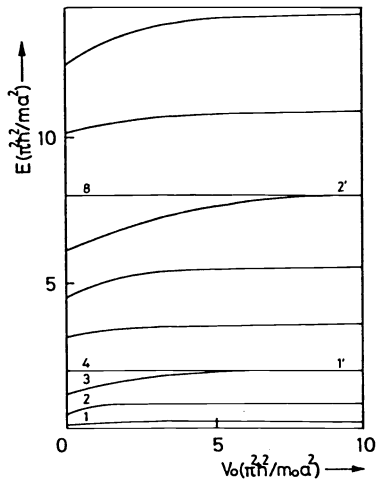


Fig. 9. Particle in the box states as a function of a δ-like perturbing potential $V_o$ at a commensurate position $x_o = a/2$.

box, new constant values for the states are obtained. For the commensurate choice of $x_o = 0.5$ shown in Fig. 9 states 4,8 etc. are not effected. They degenerate with the lower lying state and represent the state 1', 2', etc. in the separated box. The influence of more realistic defects like e.g. chain twists on the physical properties of the segments are presently under study (Ref. 30). Preliminary results for the transition matrix elements discussed in Fig. 4 of section 5 show that the general behaviour of these defects is similar to defects causing a complete interruption of the conjugation.

## 8. APPLICATIONS

Since even details of the Raman spectrum of trans-polyacetylene are basically well understood this technique provides a valuable tool to obtain information on several properties of the polymer like cis-trans isomerization dynamics, doping behaviour, degradation or electrochemical charge storage capability etc.

### Cis-trans isomerization

The irreversible cis-trans phase transition is one of the still unsolved problems of polyacetylene. It starts with an activation energy around 16 Kcal/mol and continues with about 30 Kcal/mol (Ref. 8,31). Both values are too small to allow substantial breaking of double bonds by radical generation which would be necessary for a rotational transition from the cis- to the trans-geometry. Since the Raman spectra of the cis-isomer and the trans-isomer are characteristically different a study of the spectra in the state where cis- and trans-polyacetylene are present simultaneously allows to investigate details of the phase transition. Fig. 10 shows a series of spectra obtained during a thermally induced cis-trans isomerization starting with cis-polyacetylene on the top and ending with trans-polyacetylene on the bottom. The three large peaks at 905, 1250, and 1530 $cm^{-1}$ are characteristic for the cis-polymer. The broad peak at 1100 $cm^{-1}$ and the shoulder at 1500 $cm^{-1}$ are from a small trans-fraction always present in an as prepared cis-polymer sample. Since the blue laser is in resonance for the short segments of the trans-polymer but off resonance for the cis-polymer the intensities of the corresponding lines are not directly proportional to the amount of material in the two phases. Initially only about 10% trans-polyacetylene is present. Starting isomerization the line for the C=C stretch mode grows around 1480 $cm^{-1}$ which according to Fig. 5 corresponds to fairly short segments or to an isomerization of the amorphous areas of the polymer. Only in the medium and final parts of the isomerization process the peak at 1456 $cm^{-1}$ corresponding to the crystalline part of the sample grows and finally levels off with the peak of the short segments. Thus the low values of the activation energy for the isomerization are shown to be due to an initiation of the isomerization process by defects.

The evolution of the spectra during isomerization is quite different if the process is studied with deep red laser light in the region of 6700 Å. In this case the cis-polymer is off resonance and already transparent for the exciting laser but the small amount of trans-polymer suspended in the cis-polymer matrix is still excited in resonance. The increased scattering volumen causes an enhancement of its Raman lines over the lines of the cis-polymer

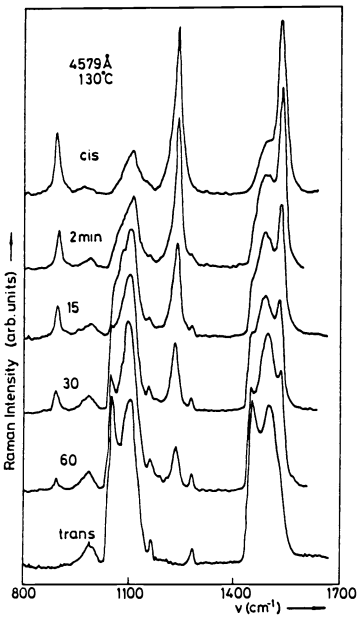


Fig. 10. Cis-trans isomerization at 130°C as observed by Raman spectra excited with 4579 Å laser light.

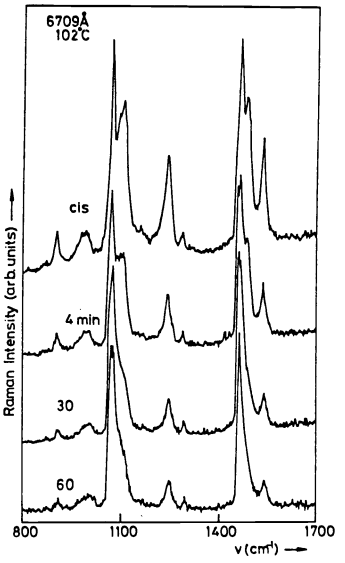


Fig. 11. Cis-trans isomerization at 102°C as observed by Raman spectra excited with 6709 Å laser light.

(Ref. 8). As an example Fig. 11 shows spectra excited with 6709 Å during an isomerization process at 102°C (Ref. 32). The resonance enhanced lines 1100 and 1470 $cm^{-1}$ are from the small amount of trans-polyacetylene in the sample. The line at 1470 $cm^{-1}$ has at least 3 peaks at 1461, 1468, and 1489 $cm^{-1}$ as can be seen e.g. from the spectrum obtained after 4 minutes isomerization. Two of the peaks probably correspond to the bimodal distribution function and the third in the center to the matching of the resonance condition. A detailed quantitative analysis of these spectra has not yet been performed.

Degradation

One possibility to learn about details of the defects interrupting the conjugation is to degrade the sample artificially. Since reaction with oxygen is probably one main reason for degradation the response of the Raman spectra of a high quality sample to an exposure to ambient conditions is interesting. Fig. 12 shows the results for an exposure up to 42 days (Ref. 33). Though the general behaviour shows the expected degradation of the sample the stability of the spectra is surprising. Even after one day exposure only very little change in the lineshape can be observed. After 42 days exposure the part of the lines comming from the short segments increased considerably but the total line for e.g. the C=C stretch mode has not yet reached a shape comparable to the one shown in Fig. 2A for a standard material. The solution of the puzzle may be due to the twofold activity of the oxygen. Oxygen can react chemically with the polymer chain to form a covalent bond and thus interrupt conjugations. On the other hand it acts as a dopand and thus oxidizes the polymer by charge transfer. In this case experiments with other dopands proved (Ref. 4,7) that the resonance conditions are weakened because electronic states are transferred from the conduction and valence band to the middle of the gap (Ref. 34). As will be shown below doping starts in the disordered areas and thus the contribution of this part of the polymer to the spectrum is weakened.

Doping

Doping polyacetylene with various oxidizing or reducing species like I, $FeCl_3$, $AsF_5$, Li, Na, etc. was extensively studied (Ref. 1). As mentioned already in Raman experiments doping always reduces the resonance effect. Another general feature is a considerable upshift of the C=C stretch mode. This effect is particularly well expressed if cis-polyacetylene is p-doped. In this case the spectra of the doped samples are characterized by weak and broad bands at positions corresponding to a highly disordered trans-polymer. Thus it was concluded that doping induces cis-trans isomerization and also a high degree of disorder (Ref. 4,35) possibly by chemical reaction of the dopand with the polymer. Applying the reversible electrochemical doping procedure and studying the change of the Raman spectra during doping in situ revealed new insights in the mechanism of the doping process. Electrochemical doping of polyacetylene is performed by dipping the polymer into an electrolyt and either short circuiting it with a counter electrode (spontaneous doping) or applying an electromotoric force between the polymer electrode and the counter electrode (Ref. 36). For a more controlled doping procedure a standard reference electrode may be used to dope the polymer at a well defined potential.

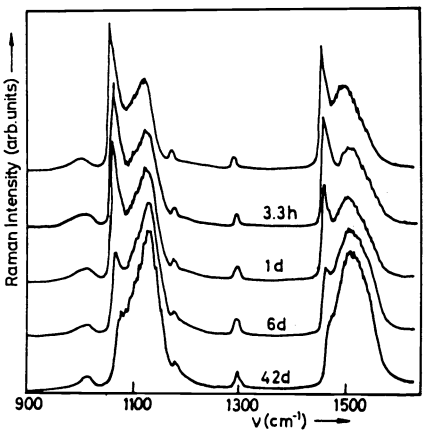


Fig. 12. Degradation of polyacetylene by exposure to air as observed by Raman spectra excited with 4579 Å laser light.

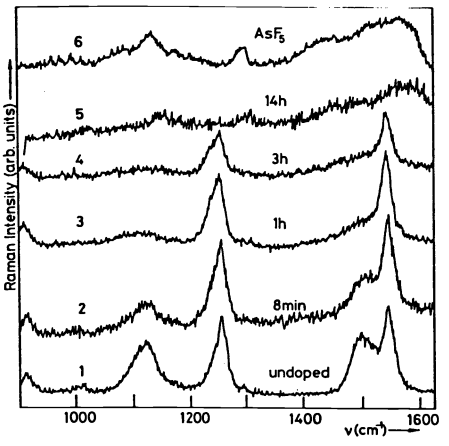


Fig. 13. Raman spectra of polyacetylene taken in situ during electrochemical doping (1-5) and after doping with $AsF_5$ (6).

To the first approach the chemical nature of the doping mechanism is regarded as identical to the mechanism for doping from the gas phase. The dopand oxidizes or reduces the polymer or, more specifically, it establishes charge neutrality for the electrochemically oxidized or reduced chain. Fig. 13 shows the change of the Raman spectra during an electrochemical p-doping process for cis-polyacetylene in an electrolyte of propylene carbonat and $LiClO_4$ (Ref. 11). Doping was performed at 3.95 V versus a Li-reference electrode. Spectrum 1 is characteristic for a cis-polymer with approximately 35% trans-content as determined from the lines at 1100 and 1500 $cm^{-1}$. With increasing doping time (spectra 2 and 3) only the lines from the trans-isomer are effected. From the peak position of these lines and from the discussion in connection with Fig. 10 and Fig. 12 we conclude that initially only the short segmented trans-part of the polymer dopes up to a saturation level. The intensity of the lines from the cis-isomer increases up to about 5% overall doping concentration. Only after continued doping (curve 4) the lines also start to decrease and finally a weak spectrum with broad lines characteristics for a highly disordered trans-polymer is observed (curve 5). It is very similar to spectra for heavily $AsF_5$-doped cis-polyacetylene (curve 6) (Ref. 4). In both cases the peak for the C=C stretch mode is upshifted to about 1570 $cm^{-1}$. According to Fig.5 this corresponds to segment lengths of 3 or 4 double bonds. The initial increase of the lines from the cis-isomer has the same origin as the enhancement of the lines from the trans-isomer in cis-polyacetylene discussed in connection with Fig. 11. Since by the doping process electronic states from the bands are transferred to the midgap position the optical absorption of the trans-part of the sample is bleached. Thus the total scattering volume is increased and the lines from the cis-isomer become stronger. The full drawn line in Fig. 14 shows the calculated behaviour of the line at 1250 $cm^{-1}$ as it is expected from a mechanism described. The symbols are experimental results. The open circuit voltage $V_{OC}$ used as abscissa is directly but nonlinearly related to the doping time and doping concentration (Ref. 37). The agreement

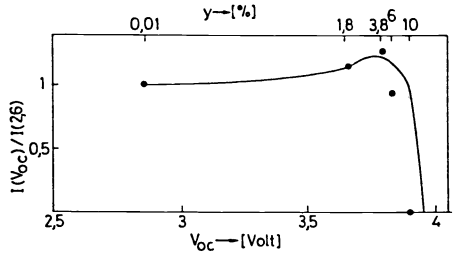


Fig. 14. Relative Raman intensity $I(V_{OC})/I(2.6)$ for the line at 1250 $cm^{-1}$ for cis-polyacetylene as a function of open circuit voltage $V_{OC}$ or doping concentration y.

Fig. 15. Raman spectra of polyacetylene taken in situ during the electrochemical undoping process (1-3) and after cyclization (4 and 5).

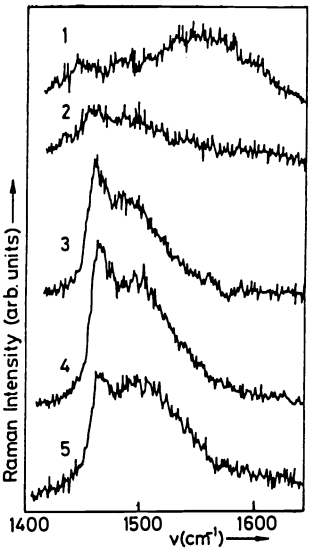

is good enough to support the suggested two phase doping mechanism. Electrochemical undoping is performed by reversing the condition for doping. Fig. 15 shows the change of the line from the C=C stretch mode during undoping. In the initial part of the process the peak of the line shifts from 1570 $cm^{-1}$ to 1460 $cm^{-1}$ where it is expected for a high quality trans-polymer sample (curves 1 and 2). About 30% of the stored charge is released during this process but no recovery of the resonance effect is observed. Only after the downshift of the line is established it starts to grow and finally takes the shape of a line in a very high quality trans-polymer (curve 3). The reversibility of the upshift and the downshift of the C=C stretch mode gives evidence that the doping induced disorder is not due to covalent chemical bonding. Rather a defect of type G in Fig. 8 may be responsible for it. By repeating the charge and discharge process the effect of cycling on the lineshape may be studied (curves 4 and 5). As can be seen, successive cycling increases the high frequency part of the peak for the C=C stretch mode and thus decreases the overall conjugation length. A detailed investigation of the effect of cycling on the Raman spectrum was recently performed by Wieners et al. (Ref. 38). It was observed that after 27 cycles a reasonable degradation of the polymer had occurred. Electrochemical doping and cycling of thermally isomerized polyacetylene was recently found by Müller et al. (Ref. 39) to give very similar results. In particular it was observed explicitly that the part of polymer with short conjugation lengths dopes first.

## 9. CONCLUSIONS

The good agreement between calculated and experimental results with respect to the lineshape and line intensity of the C=C stretch mode proves that the interruption of the conjugation by defects is the correct interpretation of the anomalous resonance Raman effect in trans-polyacetylene. This result is further supported by the strong dependence of the lineshapes on sample quality and sample treatment. Details of the shape of the distribution functions evaluated from the fit of the calculated lineshapes to the experiment must be taken with care. The bimodal character of the distribution functions is significant but the exact position and shape of the distribution of long segments is not very well defined. Physical properties for segments longer than 40 double bonds are not significantly different any more. Distribution functions of the type $P(N) \propto 1/N^x$ used in the previous calculations overestimate the short segment fraction of the polymer (Ref. 9) even if they are cut off at 3 or 4 double bonds. This is due to the strong dependence of the coupling constants $a_i$ on N.

It has been suggested to interprete the high frequency part of the C=C stretch mode as hot luminescence secondary emission of long segments only (Ref. 40). Due to the strong extrinsic nature of the emission, this explanation does not seem to meet details of the recent experimental results. Very recently Z. Vardeny et al. showed that the Raman spectra in trans-polyacetylene can be explained alternatively by assuming a distribution in the electron phonon coupling constant instead of a distribution in the conjugation length (Ref. 41). Since the localization of the electrons and their coupling to the lattice is directly related this interpretation appears to have at least the same roots as the particle in the box model described above. From the distribution P(N) of segment lengths one can immediately derive a distribution in the coupling constant a by using Eq.(14). However, in detail the coupling constant $a_i$ used in Eq.(6) and the coupling constant used in the work of Ref.41 are different.

The good understanding of the Raman spectra suggests to use the evaluated results for interpreting other physical properties of the polymer. Qualitative correlation between lineshapes of the C=C stretch mode and line widths of the ESR line has been observed. However, so far quantitative relation between these properties of the polymer was neither studied experimentally nor theoretically. Also the important question on the mechanism of the conductivity may be discussed within the prediction of the particle in the box model. First experimental results in this direction were recently reported by I. Harada (Ref. 12). It was found that samples with a low concentration of short segments yield a higher electrical conductivity after doping to saturation. This means that the crystallinity and thus band conduction plays an important role for the conduction mechanism.

Acknowledgement - The author acknowledges valuable discussion with P. Knoll, K. Iwahana, and P. Surjan. This work was supported by the Fonds zur Förderung der wissenschaftlichen Forschung in Österreich and by the Stiftung Volkswagenwerk in Germany.

## REFERENCES

1. For a review of the research in the field see Procedings of the Conferênce Internationale sur la Physique et la Chimie des Polymères Conducteurs, J. de Physique 44-C3,(1983).
2. I. Harada, M. Tasumi, H. Shirakawa and S. Ikeda, Chem. Let. 1411(1978).
3. S. Lefrant, L.S. Lichtmann, H. Temkin and D.B. Fitchen, Solid State Commumic. 29,191-196 (1979).
4. H. Kuzmany, phys. stat. sol.(b) 97, 521-531(1980).

5. F.B. Schügerl and H. Kuzmany, J. Chem. Phys. 74, 953-958 (1981).
6. L.S. Lichtmann, A. Sarhangi and D.B. Fitchen, Chem. Scripta 17, 149-150 (1981).
7. I. Harada, Y. Furokawa, M. Tasumi, H. Shirakawa and S. Ikeda J. Chem. Phys. 73, 4746-4757 (1980).
8. H. Kuzmany, E.A. Imhoff, D.B. Fitchen and A. Sarhangi, Mol. Cryst. Liquid Cryst. 77, 197-207 (1981).
9. L.S. Lichtmann, Ph.D. Thesis, Cornell University (1981).
10. S. Lefrant, E. Faulques, L. Lauchlan M.J. Kletter and S. Etemad, Mol. Cryst. Liquid Cryst. 83, 117-123 (1982)
11. P. Meisterle, H. Kuzmany and G. Nauer, Phys. Rev. B 29, 6008-6011 (1984).
12. I. Harada, Y. Furukawa, T. Arakawa, H. Takeuchi, Mol. Cryst. Liquid Cryst., to be published.
13. T. Ito, H. Shirakawa and S. Ikeda, J. Polym. Sci. Polym. Chem. Ed. 12, 11-26 (1974).
14. A. J. Epstein, H. Rommelmann, R. Fernquist, H. W. Gibson, M. A. Druy and T. Woerner, Polymer 23, 1211-1222 (1982).
15. K. Shimamura, F. E. Karasz, J. A. Hirsch and J. C. W. Chien, Macromol. Chem. Rapid Commun. 2, 473-480 (1981).
16. C. R. Fincher, C. E. Chen, A. J. Heeger, A. G. Mac Diarmid and J. B. Hastings, Phys. Rev. Lett. 48, 100-104 (1982).
17. T. C. Clarke, R. D. Kendrick and C. S. Yannoni, J. de Physique 44-C3, 369-372 (1983).
18. G. P. Brivio and E. Mulazzi, Chem. Phys. Lett. 95, 555-560 (1983).
19. H. Kuzmany, J. de Physique 44-C3 235-260 (1983).
20. L. Lauchlan, S. P. Chen, S. Etemad, M. Kletter, A. J. Heeger, A. G. Mac Diarmid, Phys. Rev.B27, 2301-2307 (1983).
21. J. Tang and A. C. Albrecht, Raman Spectroscopy, p. 33-68, Plenum Press, New York - London (1970), Ed. A. Szymanski.
22. F. Inagaki, M. Tasumi and T. Miyazawa, J. Mol. Spectrosc. 50, 286-296 (1974).
23. H. Kuzmany, P. R. Surjan and M. Kertész, Solid State Communic. 48, 243-247 (1983).
24. H. Kuhn, J. Chem. Phys. 17, 1198-1212 (1949)
25. L. Rimai, M. E. Heyde and D. Gill, J. Amer. Chem. Soc. 93, 4493-4501 (1973).
26. M. F. Granville, B. E. Kohler and J. B. Snow, J. Chem. Phys. 75, 3765-3769 (1981).
27. C. R. Fincher, M. Ozaki, M. Tanaka, D. Peebles, D. Lauchlan, A. J. Heeger and A. G. Mac Diarmid, Phys. Rev. B20, 1589-1602 (1979).
28. W. P. Su and J. R. Schrieffer, New York Nat. Acad. Sci. 77, 5626-5638 (1980).
29. K. Iwahana, unpublished.
30. P. Surjan, K. Iwahana and H. Kuzmany, unpublished.
31. T. Ito, H. Shirakawa and S. Ikeda, J. Polymer Sci., Polymer Chem. Ed. 13, 1943-1955 (1975).
32. Spectra were kindly supported by E. A. Imhoff, Cornell University.
33. P. Knoll and H. Kuzmany, Mol. Cryst. Liquid Cryst. 106, 317-329 (1984).
34. N. Suzuki, M. Ozaki, S. Etemad, A. J. Heeger and A. G. Mac Diarmid, Phys. Rev. Lett. 45, 1209-1214 (1980).
35. G. Zannoni and G. Zerbi, Chem. Phys. Lett. 87, 55-63 (1982).
36. P. J. Nigrey, D. Mac Innes, D. P. Nairns, A. G. Mac Diarmid and A. J. Heeger, J. Electrochem. Soc. 128, 1651-1657 (1981).
37. K. Kaneto, M. R. Maxfield, D. P. Nairns, A. G. Mac Diarmid and A. J. Heeger, J. Chem. Soc. Faraday Trans. I, 78, 3417-3429 (1982).
38. G. Wieners, M. Monkenbusch and G. Wegner, Bunsenberichte, to be published.
39. F. Müller, P. Meisterle and H. Kuzmany, Mol. Cryst. Liquid Cryst., to be published.
40. E. J. Mele, Solid State Communic. 44, 827-832 (1982).
41. Z. Vardeny, E. Ehrenfreund, O. Brafman and B. Horovitz, Phys. Rev. Lett. 51, 2326-2329 (1983).